Composite Structures 270 (2021) 114091

Contents lists available at ScienceDirect

Composite Structures

journal homepage: www.elsevier.com/locate/compstruct

Structural health monitoring of a CFRP structural bonded repair by using a carbon nanotube modified adhesive film

Xoan F. Sánchez-Romate [a,*], Carlos García [a,b], Joaquín Rams [a], María Sánchez [a], Alejandro Ureña [a]

[a] Materials Science and Engineering Area, Escuela Superior de Ciencias Experimentales y Tecnología, Universidad Rey Juan Carlos, Calle Tulipán s/n, 28933 Móstoles, Madrid, Spain
[b] Airbus Operations S.L., Paseo de John Lennon s/n, 28906 Getafe, Spain

ARTICLE INFO

Keywords:
Structural Health Monitoring
Carbon nanotube
CFRP repair
Strain gauge
Smart structure

ABSTRACT

Crack-sensing capabilities of a carbon nanotube (CNT) doped adhesive film have been analysed from coupon level to a composite repaired panel. Mechanical performance is not negatively affected by the addition of CNTs, due to their good distribution inside the adhesive. Moreover, the electrical resistance increases with displacement in both Single Lap Shear (SLS) and Mode-I joints, due to the combined effect of adhesive deformation and crack propagation. More specifically, Mode-I joints usually show a stick–slip behaviour with sharp increases and arrest phases in the electrical resistance, associated to changes in the failure modes. Furthermore, a structural health monitoring (SHM) test of a composite repair was carried out by different techniques such as acoustic emission, strain gauges and CNT adhesive monitoring. From electrical monitoring of the CNT adhesive, it is possible to identify some load thresholds from which the electrical resistance starts to increase. They coincide with sudden changes of the strain field monitored by the strain gauges, as well as, with sudden peaks of the sound level, being an indicative of crack nucleation, adhesive deformation and, finally, crack propagation. Therefore it highlights the great potential and robustness for on-line SHM purpose of the proposed CNT-doped adhesive films.

1. Introduction

Nowadays, there is an arising interest in the use of polymer-based composites because of their enhanced mechanical properties as well as their weight saving in comparison to conventional structural alloys. More specifically, carbon fibre reinforced plastics (CFRP) are being extensively used in several industries such as aircraft or automotive.

This extensive use comes with an increasing complexity of CFRP structures that involves the assembly of several components. In this regard, adhesive joints are a promising solution as they do not show some limitations that are present in mechanical joints such as stress concentration around the bolt holes or galvanic corrosion issues [1,2]. However, they present some limitations in terms of reliability as they are difficult to be inspected by conventional non-destructive testing (NDT) techniques in the case of complex structures. Therefore, it is necessary to develop proper inspection procedures to guarantee the mechanical performance of the adhesive joints.

In this context, the concept of Structural Health Monitoring (SHM) is gaining a great deal of attention. In fact, this concept, applied to adhesive joints, has been widely studied by using different techniques such as Fibre Bragg Grating Sensors (FBGs) or guided waves, among others [3–5]. However, these techniques usually involve complex mathematical and physical features.

In this regard, carbon nanoparticles and, more specifically, carbon nanotubes (CNTs) are now gaining attention. Besides their exceptional mechanical and electrical properties [6,7], they can be used as reinforcements in insulator matrices, allowing the creation of electrical percolation networks, leading to a drastic enhancements of the electrical conductivity of the nanocomposite [8–10]. In this regard, the SHM techniques with carbon nanoparticles are based in the measurement of the electrical conductivity between two electrodes. In fact, the presence of a damage promotes the breakage of electrical pathways, which is reflected in a sudden increase of the electrical resistivity of the material [11–13]. This fact, jointly to their piezoresistive behaviour and the tunnelling effect that takes place between adjacent nanoparticles, makes possible their extensive use as strain and damage sensors [14–18].

SHM capabilities of CNT-doped adhesive joints have been widely explored, mainly focused on paste adhesives. They have demonstrated excellent crack sensing capabilities as well as a satisfactory mechanical

* Corresponding author.
E-mail address: xoan.fernandez.sanchezromate@urjc.es (X.F. Sánchez-Romate).

https://doi.org/10.1016/j.compstruct.2021.114091
Received 8 November 2020; Accepted 6 May 2021
Available online 9 May 2021

performance due to the toughening and crack-bridging effect of the CNTs [19–24].

This study aims to analyse the crack-sensing capabilities of adhesive films, widely used in aviation, by modifying them with the addition of CNTs. In this regard, the crack-sensing and mechanical performance have been vastly explored in previous studies where an excellent agreement between mechanical behaviour and electrical response has been proved in terms of crack propagation monitoring at quasi-static [25] and dynamic conditions under fatigue tests [26] without any detriment on the overall mechanical performance of the joint. Furthermore, their SHM capabilities in more complex structures such as skin-stringer elements have been also deeply analysed [27,28].

In this context, this work is focused on a practical application such as a repair of a composite material. It constitutes a next step into the validation of the proposed adhesive for SHM purposes. In fact, the monitoring of composite bonded repairs is a subject with a great deal of attention. R.L. Rito et al. [29] used chirped fiber Bragg gratings (FBGs) for SHM of composite path repairs while G.D. Bekas et al. [30] successfully monitored the curing and damage of the same type of repairs with sensors attached to the bondline manufactured by inkjet printing of a silver nanoparticle dispersion. Both works, although interesting, do not give a complete overview about the behaviour of the composite repair, as they use external sensors. In this study, the main novelty is that the whole joint acts as a sensor, as the CNTs are dispersed inside the adhesive film.

First, the mechanical performance of CFRP standard single lap shear (SLS) and Mode-I joints manufactured by co-bonding in an autoclave have been explored, as well as, their electrical response was simultaneously measured. Here, it is important to point out that the effect of CNT addition to the adhesive film in autoclave manufactured co-bonded joints, has not been investigated yet.

Finally, a proof of concept test in a patch composite repair has been carried out. The results obtained from the electrical measurements of the CNT-doped joint have been compared with other NDT techniques such as strain gauges and acoustic emission in order to prove the potential and applicability of the CNT-adhesive film for monitoring purposes.

2. Experimental

2.1. Materials and manufacturing.

The adhesive was an epoxy-based adhesive film *FM300 k*, supplied by *Cytec*, with a wide-knit tricot carrier and a nominal thickness of 0.2 mm. Multi-wall carbon nanotubes (MWCNTs) were NC7000, supplied by *Nanocyl*. They have an average diameter of 9.5 nm and a length up to 1.5 μm.

CNT dispersion was optimized in previous studies [25,31] and consists on a ultrasonication during 20 min in an aqueous media of 0.1 wt % CNTs with 0.25 wt% of a surfactant, sodium dodecyl sulphate (SDS). Then the solution is sprayed onto the adhesive surface by using an airbrush at a pressure of 1 bar, prior to curing. The selection of the CNT to SDS ratio has demonstrated to lead to an improvement of the mechanical performance of the bonded joint.

CFRP substrates were manufactured by using a unidirectional prepreg with a carbon fiber of intermediate modulus (IMA) and a M21E epoxy resin.

2.2. Electromechanical tests on standard joints

SLS and Mode-I tests were carried out in normalized coupons following the AITM 1-0019 and AITM 1-0053 standards, respectively, with the dimensions given in the schematics of Fig. 1. Here, the joints were fabricated by a co-bonding process in an autoclave with a curing cycle of 180 °C for 8 h at a pressure of 0.9 MPa. The lay-up sequence of

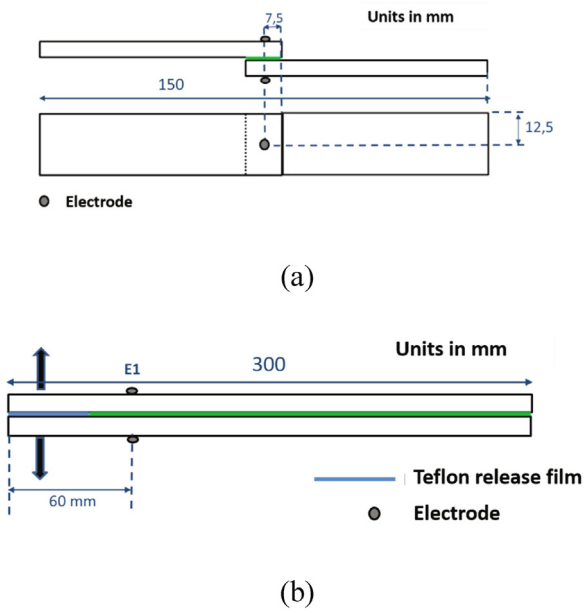

Fig. 1. Schematics of (a) SLS and (b) Mode-I standard coupon tests.

the substrates was $[0]_{11}$ and $[0]_{8}$ for SLS and Mode-I tests, respectively. Six specimens were tested for each condition.

Test rate was set as 0.5 and 10 mm/min for SLS and Mode-I tests, respectively, at room temperature in a Zwick universal tensile machine with a 10 kN load cell. Simultaneously, the electrical resistance was measured by using an *Agilent 34,410 A* module. The electrodes were placed on the outer skin of the CFRP substrates, made of copper wire and attached with silver ink to ensure a proper electrical contact. Joint dimensions and electrode disposition are shown in the schematics of Fig. 1.

2.3. Mechanical test of a composite repaired panel

Firstly, a 400 × 400 mm^2 CFRP panel was fabricated with a layer sequence of $[45/-45/90/0/90/-45/45/90/0/90/-45/45/90/0/45/-45]_s$ leading to a total thickness of 5.888 mm. Then, a scarf patch repair with a constant slope was defined in the 125 × 125 mm^2 central region of the panel (Fig. 2 (a) and (b)), affecting the last 16 plies, with a total thickness of 2.944 mm, being the ply of the base of the cone repair oriented at −45°. The rest of the plies were oriented following the same stacking sequence of the original laminate. An outer 45° ply was placed over the entire repair (Fig. 2 (c)). This repair was bonded to the base panel by using the CNT-doped adhesive film and a subsequent curing cycle by autoclave was carried out by following the same parameters of the manufacturing of the original CFRP panel (Fig. 2 (d)).

Repaired composite panel was shear tested in a tensile testing machine with a 500 kN load cell at the TEAMS S.L. facilities by using a square framework with a test rate of 0.5 mm/min (Fig. 3 (a)). Test would end by collapsing of composite panel or by reaching the maximum allowable of the testing machine.

The crack and strain monitoring of the CFRP was carried out by using eight lineal strain gauges LY41-6–350 of a nominal resistance of 350 Ω, whose disposition is shown in the schematics of Fig. 3 (b), where the front (patch repair side) and the back faces of the panel are represented. The panel corners were cut according to the required tooling for the mechanical tests.

In combination with the strain gauges, an electrical sensing scheme was defined. This electrical network was composed by five electrodes (blue circles coded E1 to E5) located as is shown in Fig. 3 (b). E1 and

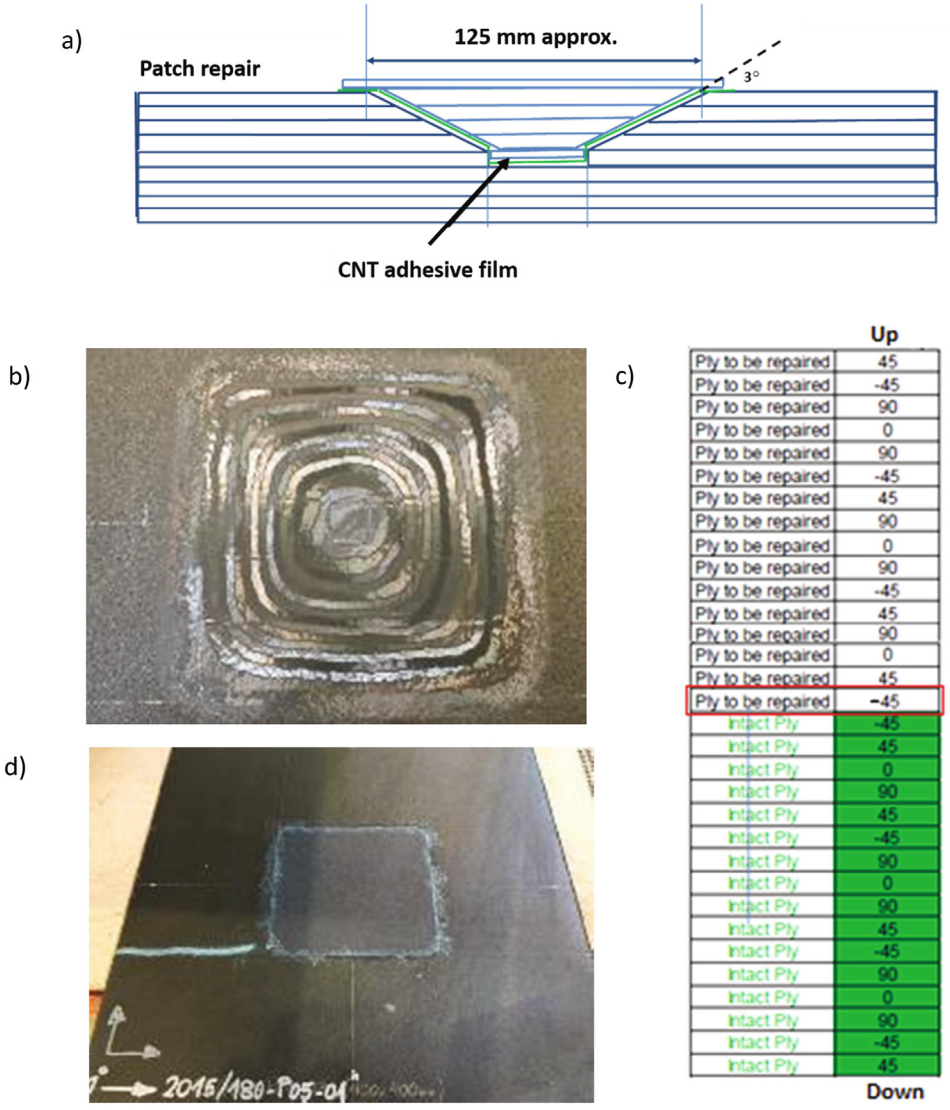

Fig. 2. Schematics of (a) patch repair, (b) scarfed dartboard prepared zone, (c) layer sequence used in the repair patch, and (d) repaired 400x400 mm coupon after autoclave curing cycle.

E3 were placed on the tensile load axis, at 10 mm from the top and bottom corners of the patch. E2 was located at the centre of the repair patch. E4 and E5 channels were placed near the right and left corners of the patch, at 10 mm, on the perpendicular line to the load axis. Electrical measurements were done through the thickness of the panel in order to record the electromechanical behaviour of the CNT-doped adhesive.

Simultaneously to the strain gauge and CNT electrical measurements, a sonometer was also positioned in the test machine in order to record the possible sounds associated to cracks or debonding, during the test. The sonometer used was a *SOUND LEVEL METER PCE-353*, with a measurement range of 30–120 dB, and a resolution of 0.1 dB.

Furthermore, an ultrasonic inspection of the repaired panel, before and after mechanical testing, was carried out to better characterize the defects. It was done by using an *AUTOMATIC EQUIPMENT TRITON 8000 TT 5 MHz* in an immersed pool.

2.4. Microstructural characterization

An analysis of the CNT distribution inside the adhesive film after curing was done by FEG-SEM characterization. It was carried out by using a *Nova NanoSEM 230* module from *Philips*. The samples were coated by sputtering a platinum layer for a proper observation.

Moreover, an analysis of the transversal section of the normalized bonded specimens was conducted by SEM analysis, using a *Hitachi S-3400 N* module. Here, the samples were properly polished and coated by sputtering a thin layer of gold.

3. Results and discussion

In this section, an analysis of electromechanical properties at coupon level is carried out for SLS and Mode-I standard joined specimens during mechanical testing. Then, a proof of concept of monitoring a patch repair is done by comparison to the other inspection techniques.

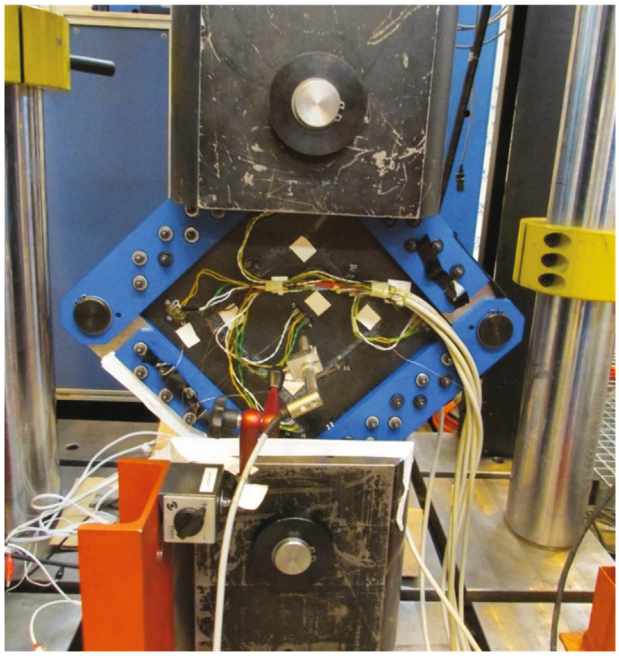

(a)

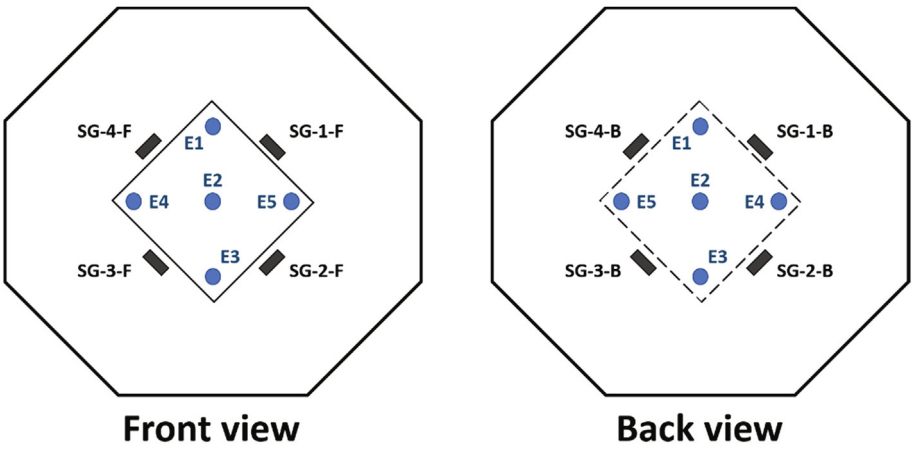

(b)

Fig. 3. (a) Experimental arrangement of the shear test of the repaired (400x400 m) composite panel and (b) schemes of the strain gauges (SG) and electric (E) sensorization of the repaired composite panel (F: front face; B: back face).

3.1. Electromechanical behaviour in standard joints

3.1.1. Mechanical behaviour of SLS and Mode-I standard joints

Table 1 summarizes the values of LSS and G_{IC} for the CNT-doped and neat adhesive joints. Here, LSS is calculated by following this expression:

$$LSS = \frac{F}{w \cdot L} \tag{1}$$

where F is the maximum load and w and L the width and the length of the overlap.

On the other hand, G_{IC} value is given by the following formula:

$$G_{IC} = \frac{A}{w \cdot a} \tag{2}$$

being A the area obtained from integrating the force–displacement curve, w the width of the specimen and a the crack length at the end of the test.

It can be observed that the mechanical behaviour of co-bonded specimens is not significantly affected by the previous addition of the CNTs at the surface of the adhesive film. This is in good agreement

Table 1
Mechanical properties of the neat and CNT-doped joints at SLS and Mode-I energy fracture tests.

Material	LSS (MPa)	G_{IC} (J/m^2)
Neat joint	39.7 ± 1.1	768.0 ± 106.7
CNT-doped adhesive	39.9 ± 0.7	775.8 ± 41.3

with previous studies in joints made by secondary bonding, where no noticeable detriment of mechanical properties was observed [25,31]. It is explained by the effect that CNTs can induce in the adhesive joint. On the one hand, CNTs promote a toughening and crack-bridging effect inside the epoxy adhesive [19] that could enhance its overall performance. However, on the other hand, the addition of the surfactant can induce a detriment of adhesive properties when interacting both the adhesive matrix and the bond interface. The combination of these two opposite effects causes that the mechanical behaviour is not significantly affected.

In this context, Fig. 4 shows several FEG-SEM images of both the cured CNT-doped adhesive film and the transversal section of the adhesive joints. Here, it is worthy to notice that, even though the CNTs are applied only superficially on the adhesive film, once completed the cycle of pressure and temperature autoclave curing, these are suitably dispersed and embedded within the epoxy adhesive (Fig. 4 (a) and (b)). This promotes the creation of effective electrical pathways through the bonded joint without inducing any prevalent aggregation of nanoparticles. Moreover, the SEM analysis of the transversal sections shows that there is no prevalent presence of porosity or voids through the joint (Fig. 4 (c) and (d)), so no overflow or entrapped air effect are observed, in opposition to the joints manufactured by secondary bonding where a prevalent porosity was observed in previous studies [25,27]. It would explain the much higher values of LSS (40 to 28 MPa) and G_{IC} (775 to 600 J/m^2) of co-bonded joints by autoclave technology in comparison to secondary-bonded joints by hot-press processing.

3.1.2. Electrical response of SLS and Mode-I standard joints

Fig. 5 shows a representative example of the electromechanical behaviour of a SLS joint during the load application. Here, it can be observed that the electrical resistance increases with the displacement. This increase can be explained by taking into account the electromechanical mechanisms that are taking place. On the one hand, the electrical resistance increases due to the adhesive deformation when subjected to an applied load. This deformation induces an increase of the interparticle distance, also called, tunnelling distance between nanoparticles. Therefore, and based on the tunnelling transport mechanisms, the electrical resistance due to tunnelling effect, which is the dominating mechanism, increases in a linear-exponential way with the increasing applied displacement, according to G. Simmons formula [32].

On the other hand, there is a prevalent crack propagation in the last stages of the SLS tests that induces a breakage of electrical pathways and, thus, a sharper increase of the electrical resistance. The combination of these commented effects leads to a highly exponential increase of the electrical resistance, especially in the last stages of the SLS test, as noticed in the electromechanical curve.

Furthermore, Fig. 6 (a) shows a representative example of the electrical response of a Mode-I joint test. Here, the prevalent mechanism is

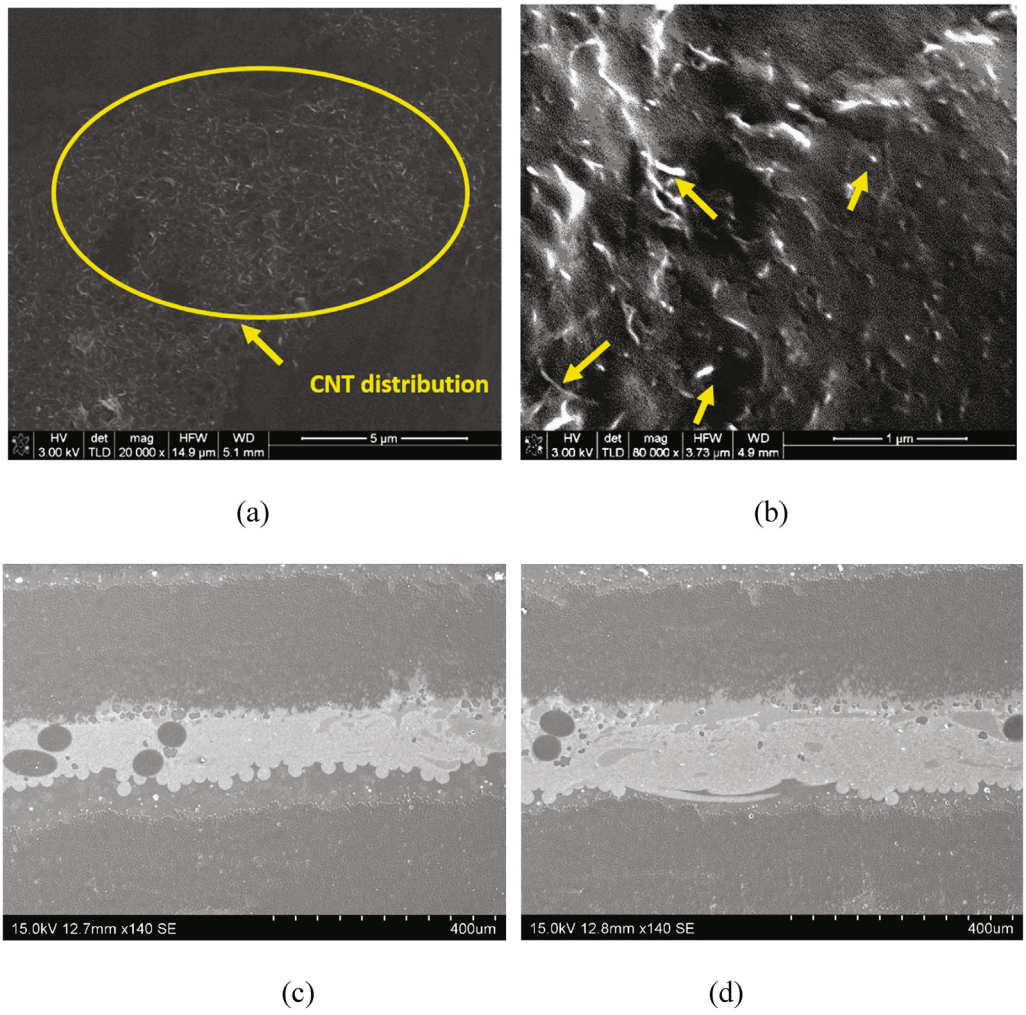

Fig. 4. FEG-SEM images of the cured adhesive showing (a) the general and (b) specific distribution of embedded CNTs, given by the yellow arrows and (c), (d) SEM images of the transversal section of the autoclave co-bonded adhesive joint.

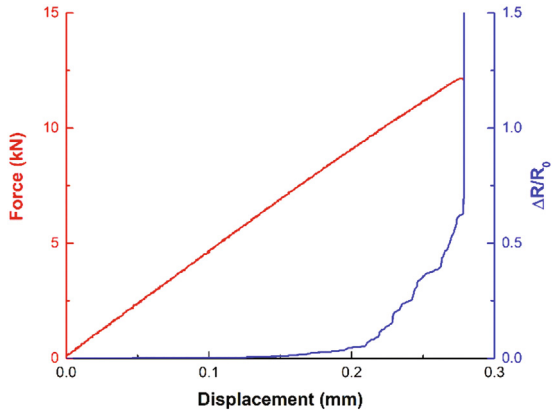

Fig. 5. Mechanical and electrical curves during a SLS joint test.

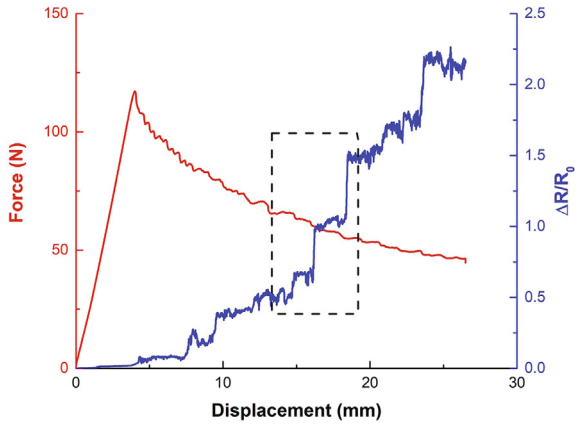

(a)

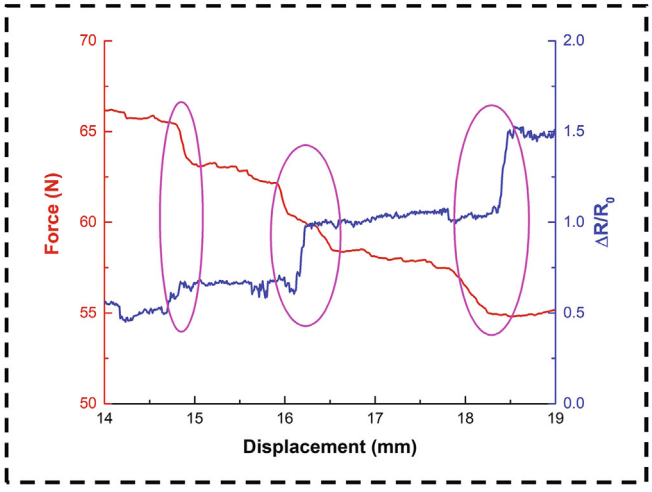

(b)

Fig. 6. Electromechanical response of Mode-I joints showing (a) the overall and (b) the detailed electrical and mechanical response (the circles represent the areas with sharp increases of the electrical response corresponding to sudden drops in the mechanical performance) and (c) fracture surfaces showing the correlation between the electrical response and crack propagation mechanisms.

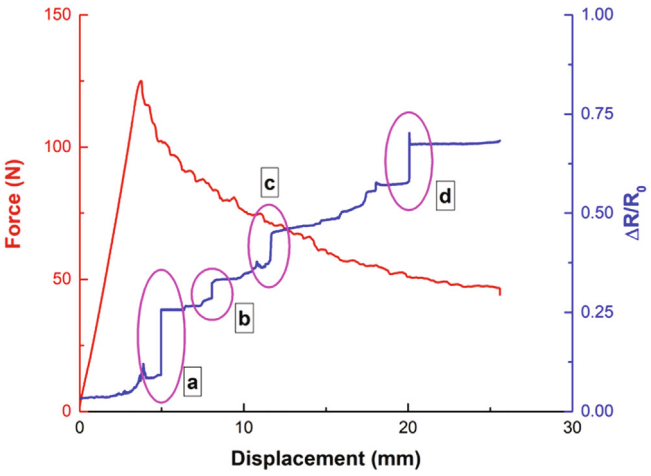

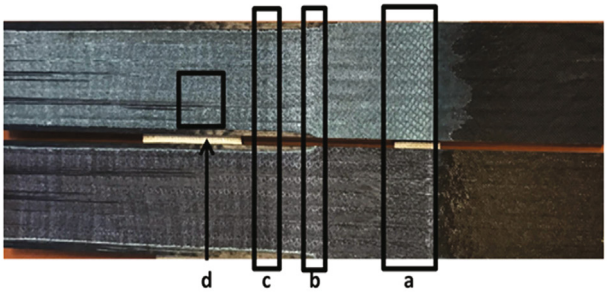

(c)

Fig. 6 (*continued*)

the breakage of conductive pathways during the crack propagation, which takes place in a more controlled way than in the case of SLS test. Therefore, when analysing the electrical response, an overall increase of the electrical resistance is observed during the Mode-I test. First, there is a soft increase of the electrical resistance, which corresponds to the initial stage of the test. Here, there is no crack propagation so the main mechanisms in this initial region is the adhesive deformation. Then, once the crack starts to propagate through the joint, it can be noticed that this increase of the electrical resistance is characterized by the alternation of sharp increases followed by arrest phases. The sharp increases are correlated to rapid crack propagation, which promotes a sudden breakage of the electrical pathways [25]. This rapid crack propagation is usually correlated to sudden drops in the mechanical load, as can be noticed in the detailed electrical response of Fig. 6 (b) where a good correspondence between the electrical and the mechanical responses can be pointed out.

Furthermore, Fig. 6 (c) shows another example of an electromechanical curve and its correspondence to the crack propagation mechanisms inside the adhesive joint. Here, it can be observed that each sudden increase of the electrical resistance corresponds to a change in the failure mechanism through the adhesive joint. More specifically, points a) and c) are correlated to a change in the failure mechanisms from an adhesive failure at the interface between the uncured substrate and the adhesive to a cohesive failure by delamination inside the uncured substrate directly. The opposite failure change is observed in points b) and d). These changes in the failure mechanisms promote a sudden breakage of the electrical pathways that is reflected in the sharp increases of the electrical resistance.

Therefore, the mechanical and electromechanical capabilities of the proposed CNT-doped adhesive film for co-bonded standard joints have been demonstrated. In this context, a proof of concept in a patch repair of a composite panel is now explored.

3.2. Structural health monitoring of a CFRP repaired composite panel

However, in order to properly understand the possible potential of the proposed technique for SHM of adhesive joint in repaired carbon fiber composite structures, it is necessary, first, to get a deeper knowledge about the health of the structure by other conventional techniques. Previously to mechanical testing, composite repaired panel was inspected by ultrasounds (Fig. 7 (a)). The results did not show neither discontinuities higher than 36 mm^2 nor volumetric porosity. Therefore, from the inspection point of view, the repair was considered valid. After mechanical testing, ultrasonic inspection was carried out again and the discontinuities and defects were characterized, allowing correlating the electrical response with the NDT results. In this regard, Fig. 7 (b) shows the results thrown by the ultrasonic inspection after the mechanical test of the repaired composite panel. Here, it can be observed the presence of two main defects: a debonding near the upper corner formed by an equilateral triangle of 10 mm side (debonding A) and a debonding near the lower corner formed by a triangle of 61 × 10 mm side.

In this regard, Fig. 8 (a) shows the electromechanical curve recorded during the mechanical test of the repaired panel, being clear the loss of linearity of mechanical response (black dotted line) for loads higher than 320–330 kN. However, by analysing the electromechanical response of the CNT-doped adhesive junction, more information can be deduced. On the one hand, channels E1 and E3 showed the highest variation of the electrical resistance, whereas channels E4 and E5 showed the lowest one. This is explained by the effect of the crack that appears in the top (E1) and bottom (E3) corner of the repair, as shown in the ultrasonic inspection. It induces a breakage of the electrical pathways that mainly affects the adjacent channels. Moreover, it can be also observed that the load threshold is different among channels (Fig. 8 (b)). E1 and E3 channels have a load threshold of around 200 kN, whereas E4 has a threshold of 250 kN and E5 channel of near 300 kN. Here, the load threshold is defined as the minimum value of the load at which a change in the electrical resistance is detected by the electric sensors.

This electromechanical behaviour can be better understood attending the crack propagation mechanisms and their effect on the electrical network. Here, an increase of the electrical resistance can be associated with two possible effects: 1) the crack nucleation and propagation, which induces a prevalent breakage of the electrical pathways inside the adhesive joints, as explained before; and 2) an excessive adhesive deformation which leads to a significant increase of the tunnelling distance between adjacent nanoparticle and, thus, to an increase of the electrical resistance of the material, as commented in the analysis of SLS joints. Here, the increase of the electrical resistance of E1 and E3 channels is motivated by the initial nucleation and, subsequent propagation of a debonding. The values of the threshold are very similar due to the symmetry of the geometry, promoting a simultaneous failure of the top and bottom corners. This symmetry is not totally reflected in the measured size of the two debonding failures, probably due to some irregularities in the repair preparation or possible misalignments that leads to a different crack propagation in the two corners aligned with the tensile load line.

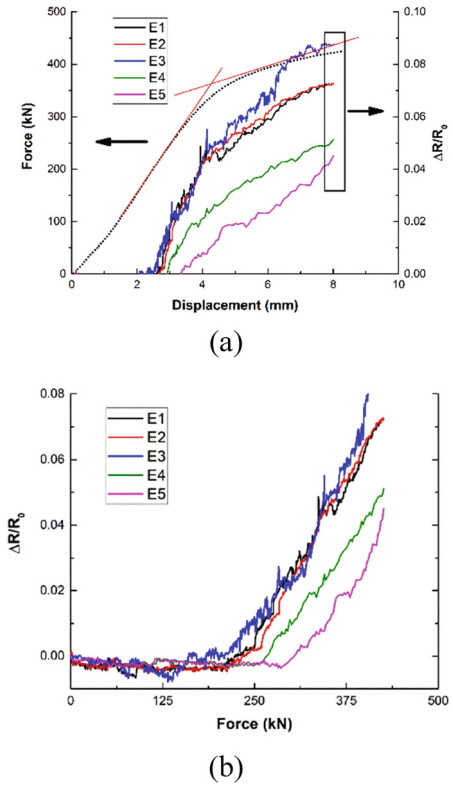

Fig. 8. (a) Electromechanical response of the repaired panel where E1 to E5 denote the CNT channels and (b) electrical resistance measurements as a function of the load.

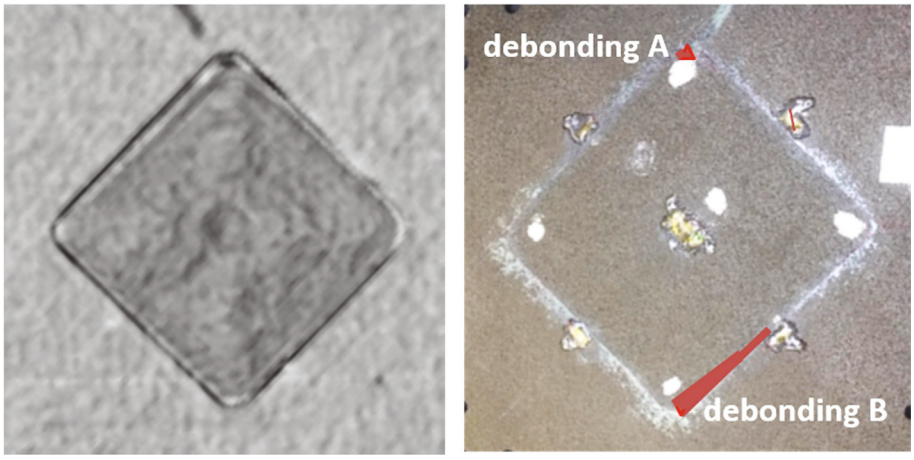

Fig. 7. Results of the ultrasonic inspection of the repaired panel (a) before and (b) after mechanical testing.

However, the electrical resistance variation associated to channels E4 and E5 cannot be explained by the effect of breakage of electrical pathways due to the presence of a crack; as no debonding has been detected just in the left and right corners of the repair patch. It must be explained accordingly to the effect that the presence of a crack can induce in the strain field of the joint as well as the presence of some micro-cracks that can appear during the test. In this regard, Fig. 9 shows the correlation between the electrical response of E5 channel and the strain measured by gauge SG-2, positioned near the electric sensor. It can be noticed that the prevalent increase of the electrical resistance of E5 is correlated to an abrupt change in the slope of the strain gauge measurements, due to the effect that the crack has on the near strain field [33]. Therefore, it is an indicative of a more prevalent adhesive deformation that would explain the increase of the electrical resistance monitored by the CNT-doped adhesive film jointly with the presence of some micro cracks that can appear due to this larger adhesive deformation.

However, although a good correlation between the electrical sensors and strain gauges measurements has been found, it is necessary to further investigate about the crack propagation mechanisms to better understand the signal given by the different SHM techniques. In this context, Fig. 10 (a) shows the results of the sound meter level test. Here, it is shown that at 282 kN, there is an abrupt increase of the sound level from the baseline of 70 dB to 79 dB. Then, a second increase to 80 dB is observed at 297 kN. Finally, three consecutive abrupt changes at 332, 337 and 334 kN of 83, 90 and 110 dB were recorded. Here, these increases in the sound level are usually associated to crack propagation mechanisms, such as matrix cracking, fibre failure, fibre/matrix or adhesive debonding [34,35].

When comparing sound level results with electromechanical signals given by the CNT electrical sensor, some interesting facts can be noticed. Firstly, it is necessary to point out that only E1 and E3 channels have been analysed, because they are the most affected by the presence of the debonding failures produced during mechanical testing. In this regard, it can be observed that there is a good agreement between the sound level test and the electrical response. E1 channel shows sudden peaks of the electrical response at 282, 337 and 344 kN (Fig. 10 (b)) corresponding to the sound level increases recorded. Therefore, here, it can be stated that, at these load values, there are prevalent debonding mechanisms. The sudden increase and subsequent decrease of the electrical resistance could be associated to the breakage of prevalent pathways and a subsequent recreation due to the closure of the crack.

Moreover, E3 channel also shows a good agreement between electromechanical curve and sound level measurements with sudden peaks of the electrical response at 282 and 344 kN (Fig. 10 (c)), indicating the load level values at which prevalent debonding mechanism are taking place. Therefore, according to these measurements, two different facts can be stated: on the one hand, the peaks in the sound level detected at 297 and 332 kN may be associated to other failure mechanisms such as fibre or matrix cracking inside the CFRP adherents, as no prevalent changes are observed in the electrical response of the these two electrical sensors. However, when analysing the load threshold of channel E5, it can be observed that coincides with the 282–297 kN sound level meter peak (Fig. 10 (d)), indicating that there can be some failure mechanisms in this region, such as micro-cracks, as stated before, that have not been detected by ultrasonic inspection. On the other hand, the initial debonding takes places at 282 kN in both the top and bottom corners of the repair. Then, the crack propagates stably, except for a peak observed at 344 kN would be indicative of a rapid crack propagation. Finally, the greatest change observed in the electrical resistance at E3 channel would be indicative of further crack

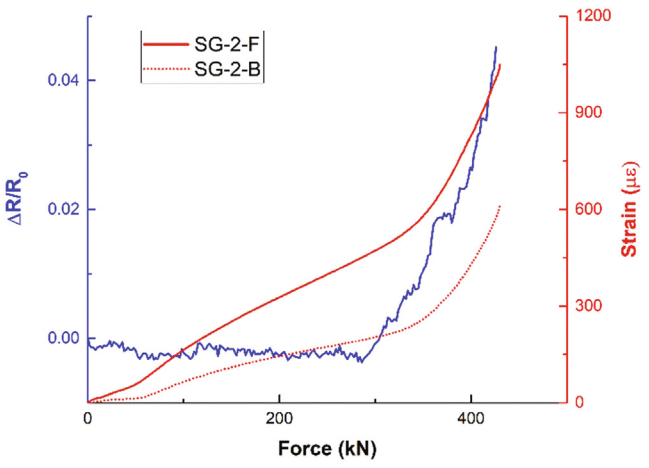

Fig. 9. Correlation between the strain measured by SG-2 strain gauge (red line) and the electrical resistance of E5 electrical sensor.

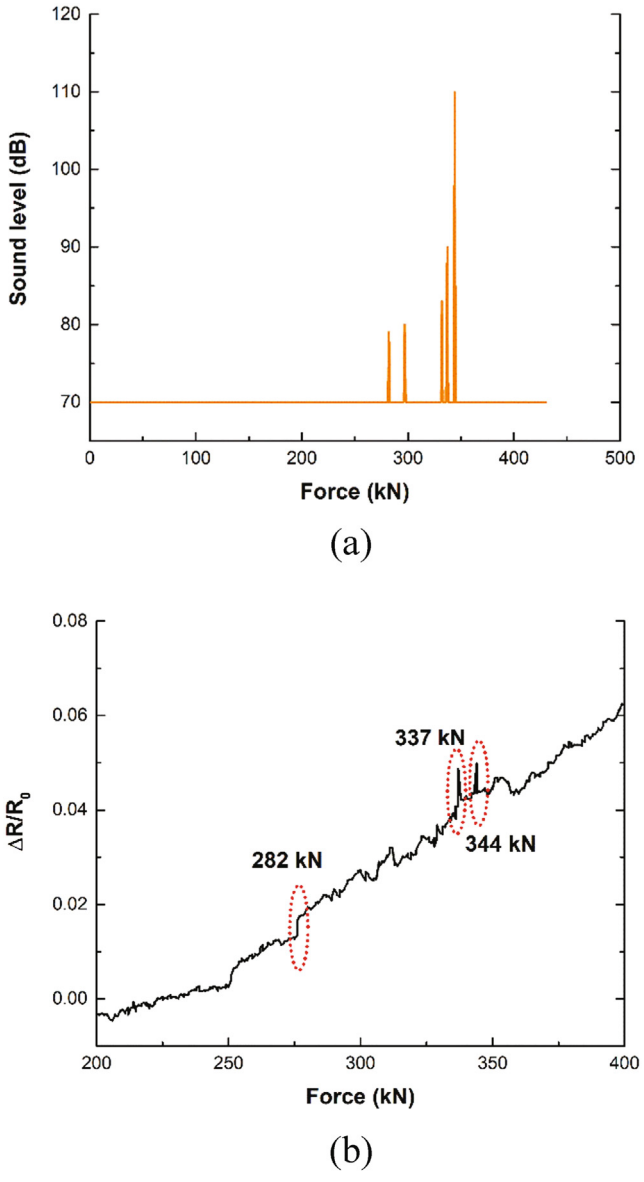

Fig. 10. (a) Results of the sound meter level tests and detailed electromechanical response of (b) E1, (c) E3 and (d) E5 channels, as well as (e) summary of detailed electromechanical response of all the CNT channels compared to the sound meter level test.

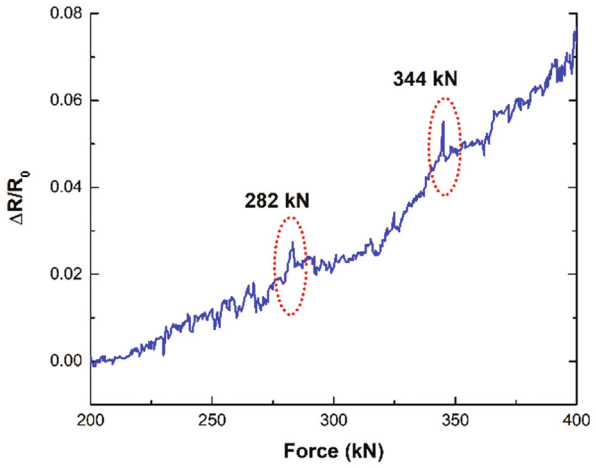

(c)

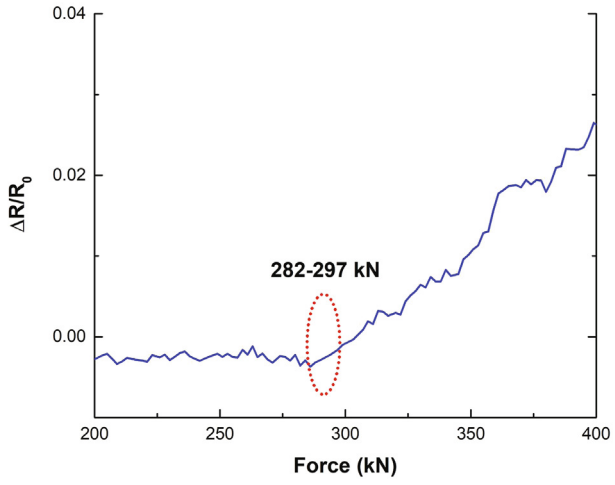

(e)

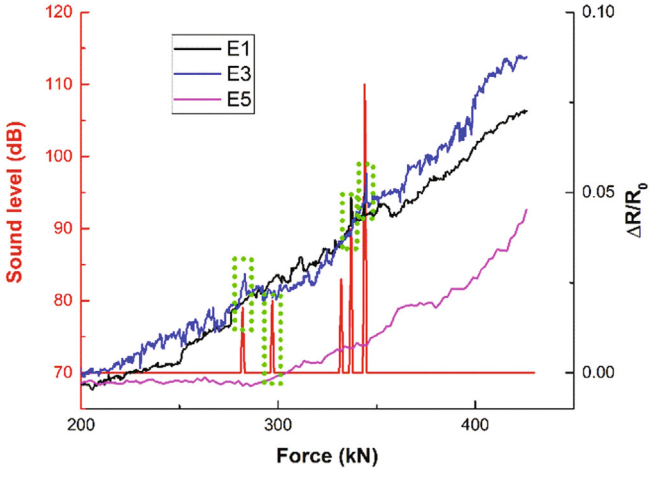

Fig. 10 (*continued*)

propagation, as previously indicated by ultrasonic inspection, where the debonded area close to the bottom corner was more extended. In this regard, Fig. 10 (e) summarizes the matches of the electromechanical resistance changes of all the CNT channels with the sound meter level tests.

Furthermore, the electrical resistance increase measured before the initial sound level peak in both E1 and E3 sensors between 200 and 282 kN can be explained by the crack nucleation taking place before the initial debonding. In fact, this is a phenomenon that has been previously reported in other studies [26] and proves the high sensitivity of the developed sensors.

Therefore, the results from the electromechanical tests from electrical sensor based on a CNT doped adhesive film show a good correspondence with the strain gauge and sound level measurements as well as with the ultrasonic inspection; proving an enormous potential and applicability for SHM purposes of composite repairs.

4. Conclusions

An analysis of SHM capabilities of a CNT-doped adhesive film has been carried out in standard coupons as well as in a composite repair.

It has been observed that the mechanical performance of the nanorreinforced joints is not negatively affected by the surface addition of the CNTs on the adhesive films with similar values of LSS and G_{IC} obtained for the neat and the modified adhesive. The electrical response, on the other hand, shows a good agreement with the mechanical behaviour. In the case of SLS joints, there is a very prevalent exponential increase of the electrical resistance, associated to both the adhesive deformation and the sudden crack propagation in the last stages of the test. In the case of Mode-I joints, the electrical resistance shows sharp increases with arrest phases, which correspond to changes in the failure mode.

The analysis of the CFRP repaired panel under shear conditions shows several interesting conclusions. On the one hand, the electrical resistance presents an initial stable phase until it starts to increase due to the effect of the crack nucleation and subsequent propagation. This increase is more prevalent in the areas where the major debonding failures takes place. On the other hand, the adjacent areas to the debonding present a much higher adhesive deformation, corroborated by the measurements of the strain gauges, that are also in good agreement with the electrical response, which starts to increase due to this effect. Moreover, the acoustic measurements also show a good correlation with the electrical response of the electrical sensor, with sudden peaks of the sound level corresponding to peaks in the electrical resistance, associated both to sudden propagation of debond defects.

Therefore, the potential and applicability of the proposed CNT doped adhesive film for SHM purposes are demonstrated for crack sensing at both normalized coupons as well as in a CFRP repair.

5. Data availability statement

The raw/processed data required to reproduce these findings cannot be shared at this time due to technical or time limitations.

Declaration of Competing Interest

The authors declare that they have no known competing financial interests or personal relationships that could have appeared to influence the work reported in this paper.

Acknowledgements

This work was supported by the Ministerio de Economía y Competitividad of Spanish Government [PROJECT PID2019-107874RB-I00] and Comunidad de Madrid regional government [PROJECT ADITIMAT-CM (S2018/NMT-4411)].

References

[1] Hussey B, Wilson Jo, editors. Structural Adhesives. Boston, MA: Springer US; 1996.
[2] Abbott S. Adhesion science: principles and practice. DEStech Publications, Inc; 2015.

[3] Bernasconi A, Carboni M, Comolli L. Monitoring of fatigue crack growth in composite adhesively bonded joints using fiber Bragg gratings. Procedia Eng 2011;10:207–12.
[4] Sherafat MH, Guitel R, Quaegebeur N, Hubert P, Lessard L, Masson P. Structural health monitoring of a composite skin-stringer assembly using within-the-bond strategy of guided wave propagation. Mater Des. 2016 JAN 2016,;15(90):787–94.
[5] Crawford A, Droubi MG, Faisal NH. Analysis of Acoustic Emission Propagation in Metal-to-Metal Adhesively Bonded Joints. J Nondestr Eval. 2018;37(2):33.
[6] Yu MF, Lourie O, Dyer MJ, Moloni K, Kelly TF, Ruoff RS. Strength and breaking mechanism of multiwalled carbon nanotubes under tensile load. Science. 2000 JAN 28 2000;287(5453):637-40.
[7] De Volder MFL, Tawfick SH, Baughman RH, Hart AJ. Carbon Nanotubes: Present and Future Commercial Applications. Science. 2013 FEB 1;339(6119):535-9.
[8] Hu N, Masuda Z, Yan C, Yamamoto Go, Fukunaga H, Hashida T. The electrical properties of polymer nanocomposites with carbon nanotube fillers. Nanotechnology. 2008;19(21):215701. https://doi.org/10.1088/0957-4484/19/21/215701.
[9] Nadiv R, Fernandes RMF, Ochbaum G, Dai J, Buzaglo M, Varenik M, et al. Polymer nanocomposites: Insights on rheology, percolation and molecular mobility. Polymer 2018;153:52–60.
[10] Chen J, Han J, Xu D. Thermal and electrical properties of the epoxy nanocomposites reinforced with purified carbon nanotubes. Mater Lett. 2019 JUL 1;246:20-3.
[11] Gao L, Chou T-W, Thostenson ET, Zhang Z, Coulaud M. Coulaud M. In situ sensing of impact damage in epoxy/glass fiber composites using percolating carbon nanotube networks. Carbon 2011;49(10):3382–5.
[12] Sánchez-Romate XF, Moriche R, Jiménez-Suárez A, Sánchez M, Prolongo SG, Güemes A, et al. Highly sensitive strain gauges with carbon nanotubes: From bulk nanocomposites to multifunctional coatings for damage sensing. Appl Surf Sci.
[13] Augustin T, Karsten J, Fiedler B. Detection and localization of impact damages in carbon nanotube-modified epoxy adhesive films with printed circuits. Structural Health Monitoring-an. International Journal. 2018;17(5):1166–77.
[14] Arif MF, Kumar S, Gupta TK, Varadarajan KM. Strong linear-piezoresistive-response of carbon nanostructures reinforced hyperelastic polymer nanocomposites. Compos A Appl Sci Manuf 2018 October;2018(113):141–9.
[15] Boztepe S, Liu H, Heider D, Thostenson ET. Novel carbon nanotube interlaminar film sensors for carbon fiber composites under uniaxial fatigue loading. Composite Structures. 2018 1 April 2018;189:340-8.
[16] García-Macías E, Rodríguez-Tembleque L, Sáez A, Ubertini F. Crack detection and localization in RC beams through smart MWCNT/epoxy strip-like strain sensors. Smart Mater Struct 2018;27(11):115022. https://doi.org/10.1088/1361-665X/aae668.
[17] Min S-H, Lee G-Y, Ahn S-H. Direct printing of highly sensitive, stretchable, and durable strain sensor based on silver nanoparticles/multi-walled carbon nanotubes composites. Compos B Eng 2019;161:395–401.
[18] Dai H, Thostenson ET. Large-Area Carbon Nanotube-Based Flexible Composites for Ultra-Wide Range Pressure Sensing and Spatial Pressure Mapping. Acs Applied Materials & Interfaces. 2019 DEC 25;11(51):48370-80.
[19] Gude MR, Prolongo SG, Ureña A. Toughening effect of carbon nanotubes and carbon nanofibres in epoxy adhesives for joining carbon fibre laminates. Int J Adhes Adhes. 2015;62:139–45.
[20] Wang Y, Raman Pillai SK, Che J, Chan-Park MB. High interlaminar shear strength enhancement of carbon fiber/epoxy composite through fiber-and matrix-anchored carbon nanotube networks. ACS Appl Mater Interfaces 2017;9(10):8960–6.
[21] Augustin T, Karsten J, Kötter B, Fiedler B. Health monitoring of scarfed CFRP joints under cyclic loading via electrical resistance measurements using carbon nanotube modified adhesive films. Compos A Appl Sci Manuf 2018 February;2018(105):150–5.
[22] Khashaba UA. Static and fatigue analysis of bolted/bonded joints modified with CNTs in CFRP composites under hot, cold and room temperatures. Composite Structures. 2018 15 June 2018;194:279-91
[23] Kumar S, Falzon BG, Hawkins SC. Ultrasensitive embedded sensor for composite joints based on a highly aligned carbon nanotube web. Carbon 2019 August;2019(149):380–9.
[24] Zhao Y, Schagerl M, Gschossmann S, Kralovec C. In situ spatial strain monitoring of a single-lap joint using inkjet-printed carbon nanotube embedded thin films. Structural Health Monitoring-an. International Journal. 2019;18(5-6):1479–90.
[25] Fernández Sánchez-Romate XX, Molinero J, Jiménez-Suárez A, Sánchez M, Güemes A, Ureña A. Carbon Nanotube Doped Adhesive Films for Detecting Crack Propagation on Bonded Joints: A Deeper Understanding of Anomalous Behaviors. ACS applied materials & interfaces. 2017.
[26] Sánchez-Romate XF, Sbarufatti C, Sánchez M, Bernasconi A, Scaccabarozzi D, Libonati F, et al. Fatigue crack growth identification in bonded joints by using carbon nanotube doped adhesive films. Smart Mater Struct. 2020;29(3):035032. https://doi.org/10.1088/1361-665X/ab7109.
[27] Sánchez-Romate XF, Moriche R, Jiménez-Suárez A, Sánchez M, Güemes A, Ureña A. An approach using highly sensitive carbon nanotube adhesive films for crack growth detection under flexural load in composite structures. Compos Struct 2019;224:111087. https://doi.org/10.1016/j.compstruct.2019.111087.
[28] Sánchez-Romate XF, Moriche R, Pozo ÁR, Jiménez-Suárez A, Sánchez M, Güemes A, et al. Monitoring crack propagation in skin-stringer elements using carbon nanotube doped adhesive films: Influence of defects and manufacturing process. Composites Science and Technology. 2020 16 June 2020;193:108147.
[29] Rito RL, Crocombe AD, Ogin SL. Health monitoring of composite patch repairs using CFBG sensors: Experimental study and numerical modelling. Composites Part A-Applied Science and Manufacturing. 2017;100:255–68.
[30] Bekas DG, Sharif-Khodaei Z, Aliabadi FMH. A smart multi-functional printed sensor for monitoring curing and damage of composite repair patch. Smart Mater Struct. 2019;28(8):085029. https://doi.org/10.1088/1361-665X/ab2d08.
[31] Sánchez-Romate XF, Jiménez-Suárez A, Molinero J, Sánchez M, Güemes A, Ureña A. Development of bonded joints using novel CNT doped adhesive films: Mechanical and electrical properties. Int J Adhes Adhes 2018 November;2018(86):98–104.
[32] Simmons JG. Generalized formula for the electric tunnel effect between similar electrodes separated by a thin insulating film. J Appl Phys. 1963;34(6):1793–803.
[33] Kashfuddoja M, Ramji M. Assessment of local strain field in adhesive layer of an unsymmetrically repaired CFRP panel using digital image correlation. Int J Adhes Adhes. 2015;57:57–69.
[34] Zhao W-Z, Zhou W. Cluster analysis of acoustic emission signals and tensile properties of carbon/glass fiber-reinforced hybrid composites. Structural Health Monitoring-an. International Journal. 2019;18(5-6):1686–97.
[35] Xu D, Liu PF, Chen ZP, Leng JX, Jiao L. Achieving robust damage mode identification of adhesive composite joints for wind turbine blade using acoustic emission and machine learning. Compos Struct 2020;236:111840. https://doi.org/10.1016/j.compstruct.2019.111840.